$\alpha-Fe_2O_3$ films grown by the spin-on sol-gel deposition method

A. Avila-García* and G. Carbajal-Franco
Sección de Electrónica del Estado Sólido,Departamento de Ingeniería Eléctrica,CINVESTAV del I. P. N.,
Av. I. P. N. No. 2508, Apartado Postal 14-740, México 07360, D. F.

A. Tiburcio-Silver
Division Posgr.,Instituto Tecnológico de Toluca-SEP,
P.O. Box 890, 50000 Toluca, Edo. Mex., México,

E. Barrera-Calva
Departamento de IPH, Area de Ingeniería en Recursos Energéticos,
Universidad Autónoma Metropolitana-Iztapalapa,
Apartado Postal 55-5340, México,D.F., México

E. Andrade-Ibarra
Instituto de Física, Universidad Nacional Autónoma de México,
Apartado Postal 20-364, México 01000, D. F.

Recibido el 17 de junio de 2002; aceptado el 8 de enero de 2003

$\alpha-Fe_2O_3$ polycrystalline films with grains larger than 31 nm were grown by the spin-on sol-gel deposition method. The particular sol used was prepared starting from two distinct precursor reagents. Both precursors leaded to similar films. Order within the films was altered by adding tin to the samples. Transmittance measurements confirmed that the hematite phase is obtained by annealing the samples above 400 °C and yielded an optical gap of about 2.2 eV, but additional transitions at 2.7 eV were also observed. From RBS measurements it was found that tin inclusion decreases iron content as expected, but also increases oxygen concentration within the films. This last observation was associated to the disorder rise when introducing tin atoms.

Keywords: Synthesis and characterization; iron oxide; sol-gel; films.

Se crecieron películas policristalinas de α-Fe_2O_3 con tamaño de grano mayor de 31 nm por el método de sol-gel, mediante un *spinner*. El sol particular usado fue preparado usando dos reactivos precursores distintos. Ambos precursores llevaron a películas similares. El orden dentro de las películas se alteró agregando estaño a las muestras. Mediciones de transmitancia confirmaron que la fase hematita se obtiene recociendo a temperaturas mayores de 400 °C y proporcionaron un ancho de banda óptico de 2.2 eV, aunque también se observaron transiciones adicionales en 2.7 eV. Mediciones de retrodispersión de Rutherford muestran que la inclusión de estaño disminuye el contenido de fierro como es de esperarse, pero también aumenta la concentración de oxígeno dentro de las películas. Esta última observación se asoció al incremento del desorden cuando se introducen los átomos de estaño.

Descriptores: Síntesis y caracterización; óxido de fierro; sol-gel; películas.

PACS: 68.60.+q; 78.65.Jd; 81.15.Lm

1. Introduction

In former works [1-3], α-Fe_2O_3 powders have been obtained from different iron salt solutions by basic precipitation. Some of these powders have been sintered to make gas sensors by the usual method. Some more researchers [4,5], have deposited the same material as thin films for either gas sensor, or fundamental studies. Some of these authors have reported results on films obtained by the sol-gel method [5]. In our approach, we assess the use of a specific sol preparation method to obtain useful iron oxide films to be used as gas detectors in the future. The spin-on sol-gel technique to deposit the films for gas sensors, was used. This particular method bears a low cost (uses small amounts of solution and the annealing temperature is not too high) and it is similar to that used by the authors in reference [6]. On the other hand, tin addition is expected to change the electrical properties of the films in a similar way than in bulk sintered material, for gas sensor usage [2]. Experimental details are given in Sec. 2, results and discussion are shown in Sec. 3 and the final conclusion is given in Sec. 4.

2. Experimental details

2.1. Sample preparation

The sol preparation method starts with an aqueous solution of an iron salt. In this experiment, we used both Ferric Nitrate and Ferrous Sulfide as the precursor salts to prepare these first aqueous solutions. Then, an iron hydroxide powder was precipitated by adding an aqueous ammonium hydroxide solution. After the powder was separated, it was peptized in acetic acid to constitute the sol required. From this sol, films can be deposited by either the spin-on or dipping techniques. In this work, spin-on at about 4500 rpm in $\sim$ 40 % humid air was selected to produce the films onto glass slide substrates. Films with six spin-on steps and intermediate drying thermal processes at about 100 °C during 15 minutes were fabricated.

Some samples were thermally treated at 150, 300, 400 and 500 °C to find the temperature at which the desired phase is obtained. Usually, a final thermal annealing process during 2 hours at 500 °C ensures that we get the hematite phase. Also, samples with 10, 30 and 50 weight percentage of tin in the solution were made by adding the appropriate amount of tin chloride to the starting aqueous solution.

2.2. Characterization

X-ray diffraction measurements were made with a Siemens D-5000 diffractometer using 1.54056 Å X-ray wavelength.

Transmittance measurements were taken with a Shimadzu UV-2401PC spectrophotometer in the range from 200 nm to 1100 nm wavelength.

The Atomic Force Microscope images were obtained with a CP-ambient model of Park Scientific Instruments.

RBS measurements were done by using an ≈ 4 μC dose of 2.6 MeV alfa particles accelerated by a 5.5 MV Van de Graff generator.

3. Results and discussion

3.1. X-ray diffraction

X-ray diffraction patterns of solids coming from the two precursor solutions are presented in Fig. 1. Results from samples coming from Ferric Nitrate are labeled Ac[1] and those from Ferrous Sulfate are labeled Ac[2]. The small triangles correspond to the values established for α-Fe_2O_3 in a standard card as given by the JCPDS-ICDD pattern. Only the main peaks are labeled. The spectra of samples from both precursors used, agree with the hematite standard corresponding to the α phase of iron oxide. As said before, the thermal treatment is the same for both. When calculated from the (104) peak of the Ac[1] spectrum, the grain size turned out to be at least of 31 nm, about 20% larger than that for Ac[2].

We see that as the tin content increases, the hematite peaks tend to decrease, indicating that the nano-crystalline structure vanishes, becoming the solid an amorphous material. None alternate arrangement is produced by the introduction of tin in the hematite matrix, only destroying order. This allows to control the microstructure of the films.

3.2. Optical measurements

Transmittance measurements of films that underwent heat treatments at increasing temperatures (150, 300, 400 and 500 °C) are shown in Fig. 2a as a function of the wavelength. It is seen that as the annealing temperature increases, a steeper optical edge is better defined. Also, a second fast

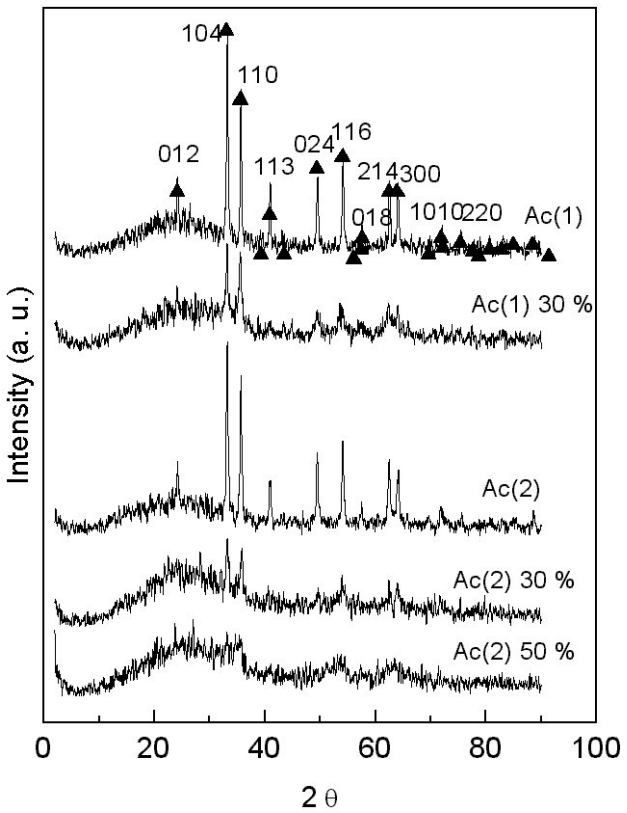

FIGURE 1. X-ray diffraction spectra of powders obtained starting from the two precursor salts mentioned in the text, also showing the effect of incorporating different tin content.

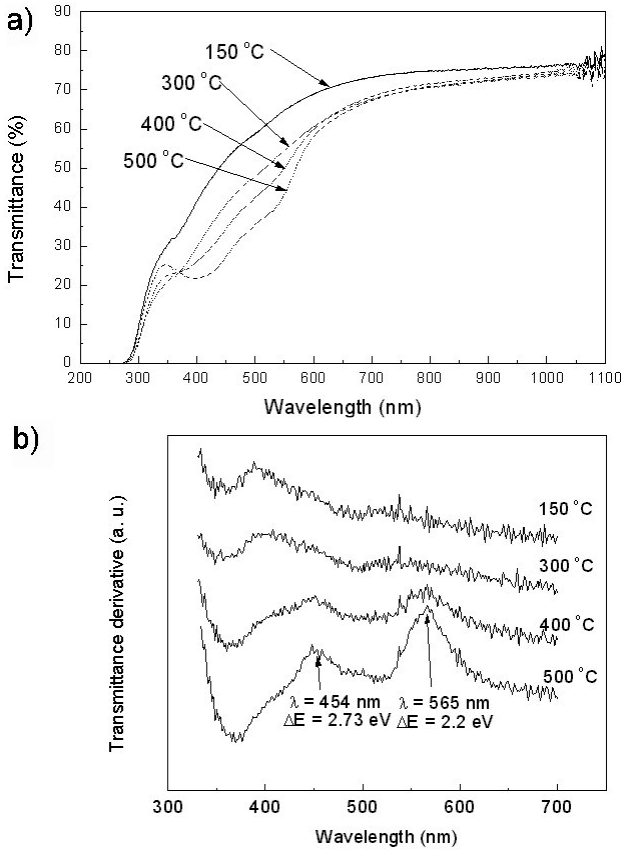

FIGURE 2. a) Transmittance spectra of four films thermally annealed at 150, 300, 400 and 500 °C. b) Wavelength derivative of the transmittance spectra, near the region of the absorption edge.

transition can be noticed at shorter wavelength. A simple estimate for the optical gap can be given by assuming that its value is near the point where the transmittance variation is the fastest one. Thus, this value can be approximately given as the energy corresponding to the point where the wavelength derivative gets a maximum. This derivative was numerically calculated for the plots in Fig. 2a and it is shown in Fig. 2b. For the sake of clarity, these curves were vertically shifted. Two local maxima can be seen in the curves corresponding to 400 and 500 °C. The position of these maxima is practically the same in both curves, which is indicative of no further important changes. This was confirmed by another sample on quartz, annealed at 900 °C, which is not shown. By taking the wavelengths of the two local maxima in this plot as 565 nm and 454 nm, we calculate the corresponding photon energies as 2.2 eV and 2.73 eV, respectively. The first value corresponds closely to the optical gap energy given in Ref. 7 for Fe_2O_3. Since both maxima evolve similarly while the hematite phase is formed and in view that no other phase is found from the X-ray measurements, the second local maximum should be ascribed to some feature of the dispersion relationship of this material.

The hematite structure is achieved when the temperature reaches 400 °C, but is best defined for 500 °C. These results agree well with the results of X. Q. Liu *et al.* [3] who achieved the same phase by annealing between 450 and 500 °C. In Fig. 2b, two bumps can be seen in the plot of 150 °C. The first is peaked slightly below 400 nm and the second near 525 nm. As this annealing temperature is low, they should be correlated to the existence of a large amount of OH^- species in the film. This is consistent with the fact that they tend to vanish while the chemical transformation of these radicals produce an oxide and the main peaks related to the α-Fe_2O_3 phase are better defined as the annealing temperature is increased.

3.3. Atomic force microscopy

Images of films with the same thermal treatment (500 °C during 2 hours) but distinct content of tin are shown in Figs. 3 and 4. In Fig. 3 a clear difference between the surface structure of the sample without and that with 30% of tin is seen. In Fig. 4 this difference is not as clear as in the previous case, but also the three-dimensional structures tend to be smoother with the tin content, indicating that atomic arrangement vanishes. This can be confirmed by noting the vertical scales in both figures: although the difference between the highest features is not so large (0.91 μm and 1.04 μm), this difference will certainly determine a corresponding difference in the calculated roughness of the film surface. This fact agrees well with the XRD patterns shown above.

3.4. RBS measurements

The chemical composition of the films was studied by the well known RBS technique. A typical graphical representa-

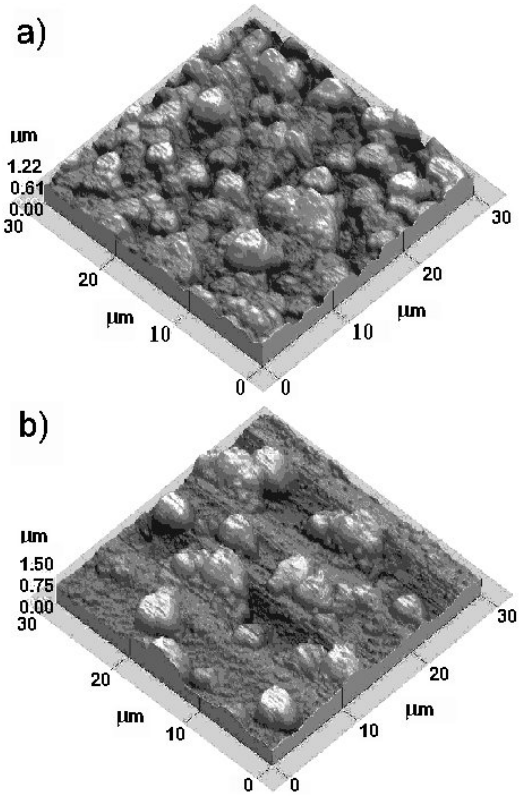

FIGURE 3. AFM images of films coming from nitrate precursor a) without tin. b) with 30% content of tin.

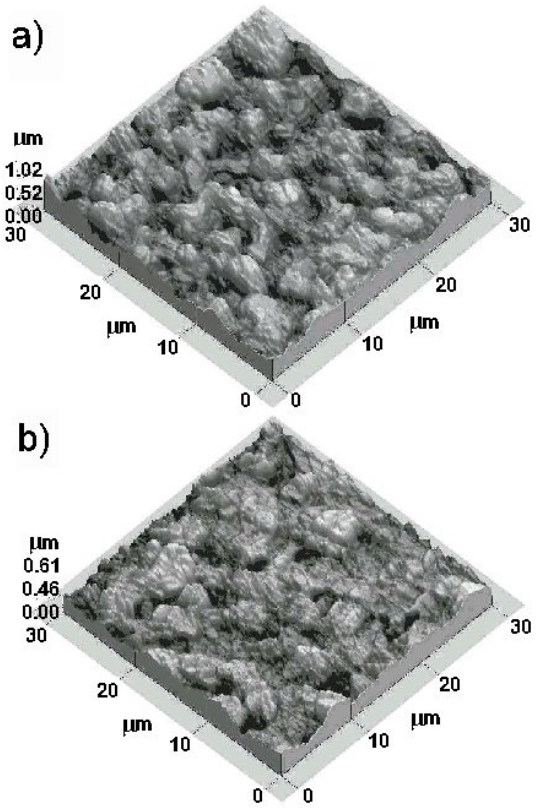

FIGURE 4. Micrographs of films from sulfate precursor, a) with 30% of tin, b) with 50% of tin.

tion of the results is shown in Fig. 5a, where a theoretical model fitting can be seen. This result corresponds to a film-substrate system where layer 1 stands for the hematite film and layer 2 for the glass substrate. The atomic fractions of iron and oxygen shown for layer 1 correspond precisely to the hematite stoichiometry. After fitting the experimental results from other samples, the plot in Fig. 5b can be drawn to illustrate how tin inclusion modifies the iron and oxygen contents. As the tin content increases, iron incorporates in less concentration within films from both precursors but at the same time, large amounts of oxygen are also incorporated. Although tin inclusion destroys order in the film, and consequently large crystals are no longer built, we can assume that tin atoms bind to oxygen to fulfill its bonding requirements. From the above said and according to Fig. 5b, a part of the oxygen detected should exist as adsorbed ions onto the film surface. It is well known that oxygen is adsorbed by the film surface, following the reaction [8]:

$$O_{2_{gas}} \leftrightarrow O_{2_{ad}} \leftrightarrow O^{-}_{2_{ad}} \leftrightarrow O^{-}_{ad} \leftrightarrow O^{2-}_{ad} \leftrightarrow O^{2-}_{latt},$$

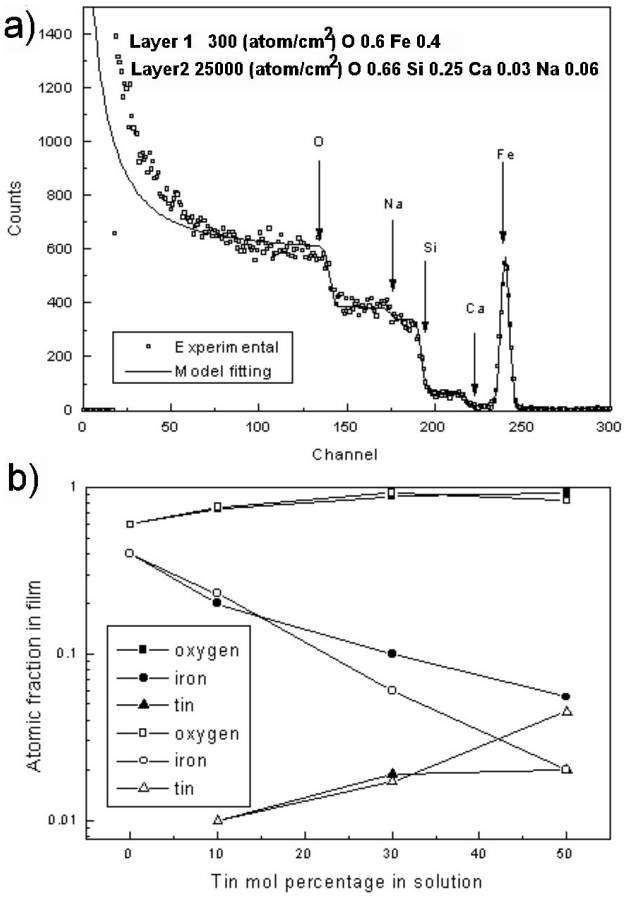

FIGURE 5. a) Typical RBS plot used to identify the masses of components backscattered, corresponding to a sample from precursor Ac[1] without tin. b) Atomic fraction of the film components as a function of the tin content added during solution preparation. Solid symbols correspond to samples from precursor Ac[1], open symbols to films from precursor Ac[2].

where the sub-indices gas, ad and latt stand for gaseous, surface adsorbed and lattice oxygen, respectively. Furthermore, oxygen atoms ionize by taking free electrons from the film, then changing the corresponding conductivity.

If we use the experimental atomic fraction ratio [Fe]/[Sn] to find the corresponding molecular ratio $[Fe_2O_3]/[SnO_2]$ in the films, oxygen in molecular configuration can be estimated and the remaining oxygen should be the above mentioned adsorbed oxygen. After doing the proper calculations, results can be plotted in Fig. 6. As the calculated amount of oxygen in Fe_2O_3 and SnO_2 molecules does not change appreciably with tin inclusion, it turns out that the total oxygen variation is due practically all to surface adsorption. This can be understood in terms of the increasing disorder as the tin content increases, which produces smaller grain size and an increasing surface/volume ratio due to the creation of an increasing number of grain boundaries not only on the surface but also within the film bulk.

4. Conclusion

By using the sol-gel spin-on method outlined with the specific sol prepared, nano-crystalline hematite films were obtained with grain size larger than $\sim$ 31 nm. Both reagents used to prepare the sol leaded to similar results. As tin is introduced in the starting solution in high concentrations between 10% and 50%, this crystalline arrangement vanishes, leading towards amorphous films. This is confirmed by the observation of some AFM images. Hence, the structure of the films can be controlled by introducing the proper amount of tin. The effect of the annealing temperature was studied by means of transmittance measurements. It was found that the hematite structure is achieved by using temperatures between 400 °C and 500 °C as reported in former works. Also, the optical gap was found to be 2.2 eV and an additional feature in the band structure of this material at 2.7 eV was observed. This could correspond to valence band splitting, but should be confirmed with complementary measurements. The Fe

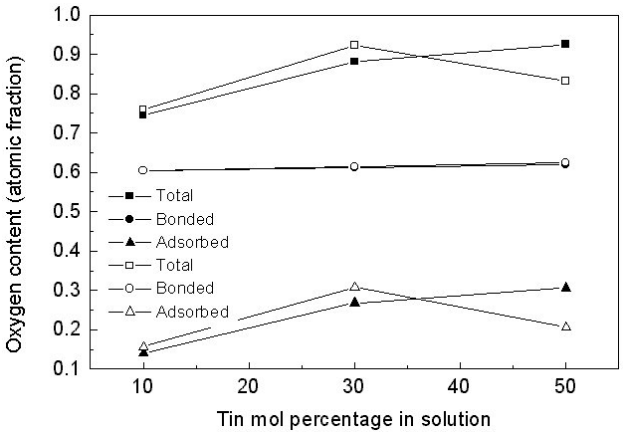

FIGURE 6. Oxygen content detected in the different films. Solid symbols correspond to samples from precursor Ac[1], open symbols to films from precursor Ac[2].

and O atomic fraction for the hematite phase within films without tin was confirmed by RBS measurements. Additional information from RBS experiments was obtained: as tin is incorporated into the films, the iron content decreases, suggesting substitutional incorporation and besides, the amount of oxygen is increased. This can be ascribed to a much higher amount of oxygen that is adsorbed in the increasing surface area due to the disorder rise. This is important for sensor applications particularly. Hence, the deposition method used here allows deposition of films that are potentially useful for sensor applications.

Acknowledgements

We gratefully acknowledge to M. Sc. Rogelio Fragoso and to Eng. Marcela Guerrero for providing the AFM images and the XRD patterns, respectively. Also, we thank, E.P. Zavala and J.C. Pineda for support in using the nuclear techniques based on the 5.5 MV Van de Graff accelerator, whose performance is financially supported by project DGAPA-UNAM IN108798. Also, this work was mainly supported by the project No. 27202A of CONACYT, Mexico.

∗. Corresponding author.

1. Y. Nakatani and M. Matsuoka, *Jap. J. of Appl. Phys.* **21** (12) (1982) L758.
2. Y. Nakatani, M. Sakai and M. Matsuoka, *Jap. J. of Appl. Phys.* **22** (6) (1983) 912.
3. X.Q. Liu, S.W. Tao, and Y.S. Shen, *Sensors and Actuators B* **40** (1997) 161.
4. L. Armelao *et al., J. Of Non-Cryst. Solids* **192-193** (1995) 435.
5. P. Chauhan, S. Annapoorni and S.K. Trikha, *Thin Solid Films* **346** (1999) 266.
6. E. Barrera, T. Viveros, A. Avila, P. Quintana, M. Morales and N. Batina, *Thin Solid Films* **346** (1999) 138.
7. H.L. Tuller in *Nonstoichiometric oxides*, O. Toft Sorensen (Ed.) (Academic Press, Roskilde, Denmark, 1981).
8. K. Hara and N. Nishida, *Sensors and Actuators B* **20** (1994) 181.